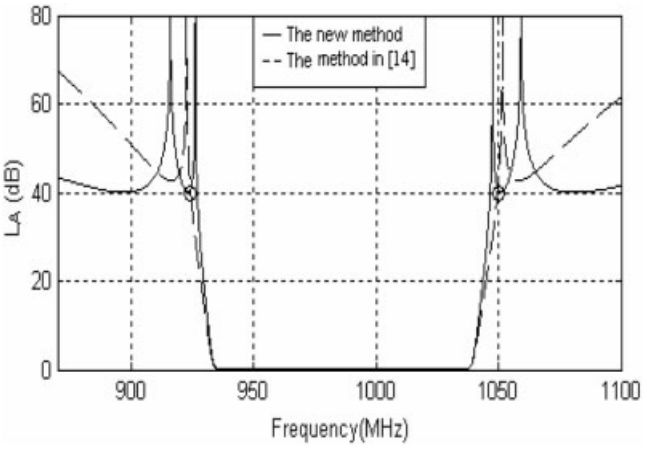

Figure 6 The comparison of the practical filter insertion loss, the circle is the specifications

filter design.

[Example 3] The given bandpass filter specifications are [14]:

The centre frequency is $f_0 = 985$ MHz.
The fractional bandwidth is FBW = 0.10359.
The return loss in the passband is RL = 20 dB.
40 dB rejection bandwidth is 125.5 MHz.

1. The normalized frequencies are $\omega_1 = \pm 1.2300$ rad/s ($L_{A1} = 40$ dB).
2. According to the filter specifications and (7) the traditional filter degree is 12.
3. In [14], the filter degree is 8 and the number of transmission zeros is 2, which are shown in Table 5.
4. In terms of the method in this paper, the filter degree is 7 and the number of transmission zeros is 4, which are shown in Table 5.

By applying the frequency transformation from a lowpass prototype to a practical bandpass filter, the comparison of the practical filter insertion loss between the traditional method, the method in [14], and the new method is shown in Figure 6. From Table 5 and Figure 6, we know that the new method is effective in the bandpass filter design. Tables 6 and 7 show the expressing of coefficient a for $k = 3$ and 4, respectively.

5. CONCLUSIONS

The general Chebyshev filter has been widely used in modern communication because of the excellent performance. This article presents a new method, which can determine the filter degree and transmission zeros simultaneously. The filter designed by this method has the least degree and the optimum position of transmission zeros. This method will shorten the circle of the design, and be useful for the practice.

ACKNOWLEDGMENT

This work is supported by the Science Fund of China (No. 60171011) and (No. 60571056).

REFERENCES

1. A.E. Atia and A.E. Williams, Narrow-bandpass waveguide filters, IEEE Trans Microwave Theory Tech 20 (1972), 258–265.
2. A.E. Atia, A.E. Williams, and R.W. Newcomb, Narrow-band multiple-coupled cavity synthesis, IEEE Trans Circuit Syst 21 (1972), 649–655.
3. R.J. Cameron, Fast generation of Chebyshev filter prototypes with asymmetrically-prescribed transmission zeros, ESA J 6 (1982), 83–95.
4. R.J. Cameron, General coupling matrix synthesis methods for Chebyshev filter function, IEEE Trans Microwave Theory Tech 47 (1999), 433–442.
5. R.J. Cameron, Advanced coupling matrix synthesis techniques for microwave filters, IEEE Trans Microwave Theory Tech 51 (2003), 1–10.
6. R.J. Cameron, General prototype network synthesis methods for microwave filter, ESA J 6 (1982), 193–206.
7. R.J. Cameron and J.D. Rhodes, Asymmetric realizations of dual-mode bandpass filter, IEEE Trans Microwave Theory Tech 29 (1981), 51–58.
8. R. Levy, Filters with single transmission zeros at real and imaginary frequencies, IEEE Trans Microwave Theory Tech 24 (1976), 172–181.
9. R. Levy, Direct synthesis of cascaded quadruplet (CQ) filters, IEEE Trans Microwave Theory Tech 43 (1995), 2940–2944.
10. R. Hershtiong, R. Levy, and K. Zaki, Synthesis and design of cascaded trisection (CT) dielectric resonator filters, Eur Microwave Conf, Jerusalem, Israel (1997), 748–791.
11. W.A. Atia, K.A. Zaki, and A.E. Atia, Synthesis of general topology multiple coupled resonator filters by optimization, IEEE Microwave Theory Technology Digest, Baltimore, 1998, pp. 821–824.
12. S. Amari, Synthesis of cross-coupled resonator filters using an analytical gradient-based optimization technique, IEEE Trans Microwave Theory Tech 48 (2000), 1559–1564.
13. R. Ye and Q.X. Chu, Extraction of finite transmission zeros of general Chebyshev filters, 4th International Conference on Microwave and Millimeter Wave Technology, Beijing, 2004, pp. 26–28.
14. J.S. Hong and M.J. Lancaster, Microstrip filters for RF/microwave application, Wiley, New York, NY, 2001, pp. 322

SIMULTANEOUS NOISE AND INPUT MATCHED ULTRA WIDE BAND LNA DESIGN

Yuna Shim, Chang-Wan Kim, and Sang-Gug Lee

Received 22 February 2007

ABSTRACT: *Proposed a low noise amplifier (LNA) design technique that satisfies simultaneous noise and input matched condition over ultra wide band (UWB) frequency range. Simultaneously, noise- and input-matched UWB LNA is implemented in 0.18 μm CMOS technology, and measurements show higher than 8 dB of input return loss, maximum gain of 10.5 dB, and noise figure of 3.9–6 dB over 2–4 GHz while dissipating 4 mA from a 1.8-V supply.* © 2007 Wiley Periodicals, Inc. Microwave Opt Technol Lett 49: 2275–2279, 2007; Published online in Wiley InterScience (www.interscience.wiley.com). DOI 10.1002/mop.22650

Key words: *low noise; ultra wideband; RF amplifier; LNA*

1. INTRODUCTION

Ultra wide band (UWB) transceivers are drawing attention for high data rate radio applications. As a key element for the radio transceiver, the UWB LNA warrants a number of design challenges, such as wide band input matching, a sufficient/constant power gain, low power, high linearity, and low noise figure (NF). With narrow band LNA, the simultaneous noise and input matching (SNIM) technique [1] are popular to minimize the NF. However, the SNIM, in principle, can be satisfied only at a single frequency. The UWB LNA design technique that satisfied the SNIM condi-

tion has yet been reported. This article presents an LNA design approach that achieves SNIM over the limited range of frequencies but still ultra wide-band, e.g., 3–5 GHz range.

2. UWB LNA DESIGN

Figure 1 shows the cascode amplifier topology, which is popular for the SNIM technique-based narrow band LNA design, where v_{in} represents the input signal and V_B the dc biasing. For the amplifier shown in Figure 1, the input impedance (Z_{in1}) and the optimum source impedance (Z_{opt1}) are given in [1]

$$Z_{in} = \frac{g_m L_s}{C_{gs}} + sL_s + \frac{1}{sC_{gs}}, \tag{1}$$

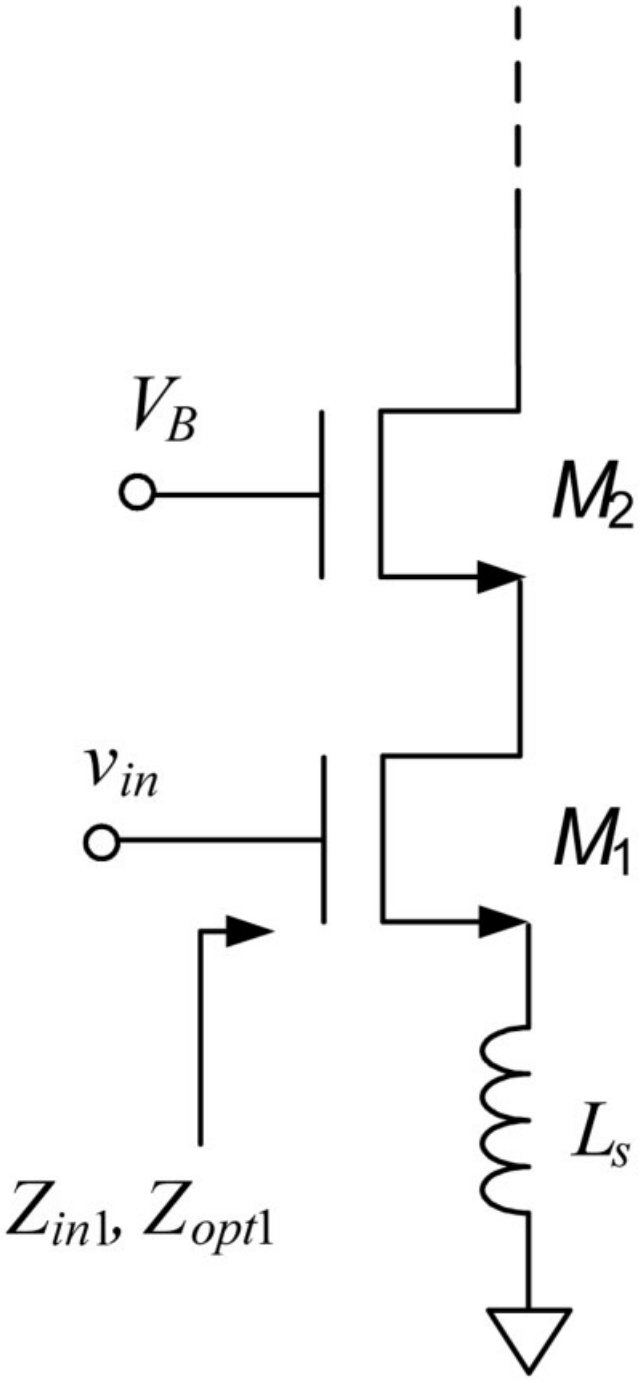

Figure 1 A cascode amplifier with inductive source degeneration

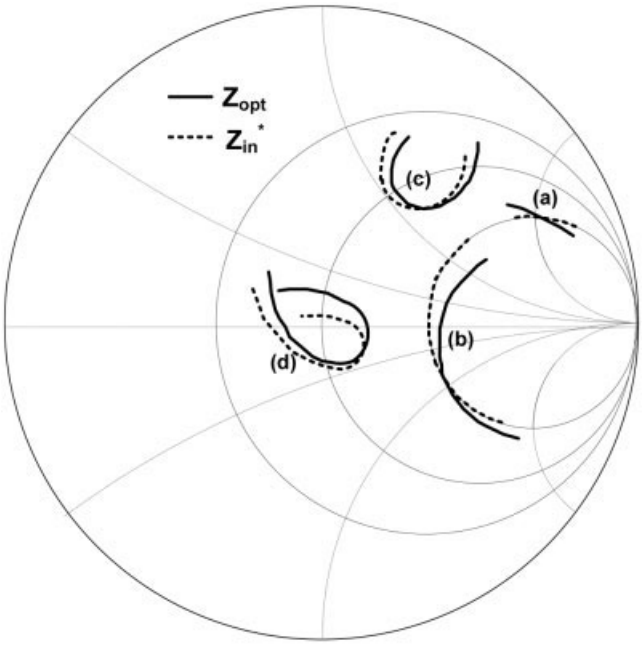

Figure 2 Optimum source impedance and the complex conjugate input impedance of the LNA for the frequency range of 3–5 GHz. (a) Z_{in1} and Z_{opt1} (b) Z_{in2} and Z_{opt2} (c) Z_{in3} and Z_{opt3} (d) Z_{in4} and Z_{opt4}

$$Z_{opt} = \mathrm{Re}[Z_{opt}^o] - m\frac{1}{sC_{gs}} - sL_s, \tag{2}$$

respectively, where

$$\mathrm{Re}[Z_{opt}^o] = \frac{\alpha\sqrt{\dfrac{\delta}{5\gamma(1-|c|^2)}}}{\omega C_{gs}\left\{\dfrac{\alpha^2\delta}{5\gamma(1-|c|^2)} + \left(1+\alpha|c|\sqrt{\dfrac{\delta}{5\gamma}}\right)^2\right\}}, \tag{3}$$

g_m and C_{gs} the transconductance and gate-source capacitance of transistor M_1, respectively, L_s the degeneration inductance, and m, α, δ, γ, and c are the constants. The simultaneously noise- and input-matched LNA design requires the condition of the complex conjugate of Z_{in1} being equal to Z_{opt1} ($Z_{in1}^* = Z_{opt1}$). From (1) and (2), with technology scaling, the imaginary components of Z_{in1}^* and Z_{opt1} are nearly equal as m approaches 1. Therefore, to satisfy SNIM, the values of g_m, C_{gs}, and L_s have to be chosen to make $\mathrm{Re}[Z_{in1}^*] = \mathrm{Re}[Z_{opt1}]$. From (1), (2), and (3), $\mathrm{Re}[Z_{opt1}]$ is inversely proportional to the frequency whereas $\mathrm{Re}[Z_{in1}^*]$ is not. Therefore, in principle, the SNIM can be satisfied only at one frequency, which limits the technique to the narrow band design.

In the Smith Chart shown in Figure 2, the two curves labeled by (a) represents the Z_{in1}^* (dashed line) and Z_{opt1} (solid line) of the LNA shown in Figure 1, respectively. Figure 2(a) shows the simultaneously noise- and input-matched condition at 4 GHz. In Figure 2(a), Z_{in1}^* and Z_{opt1} are equal at 4 GHz and diverges with

TABLE 1 Z_{in1}^* and Z_{opt1} of the Cascode Amplifier Shown in Figure 1

	3.0 GHz	4.0 GHz	5.0 GHz
Z_{in1}^*	$130 - j280$	$125 - j215$	$120 - j175$
Z_{opt1}	$140 + j275$	$120 + j195$	$105 + j150$

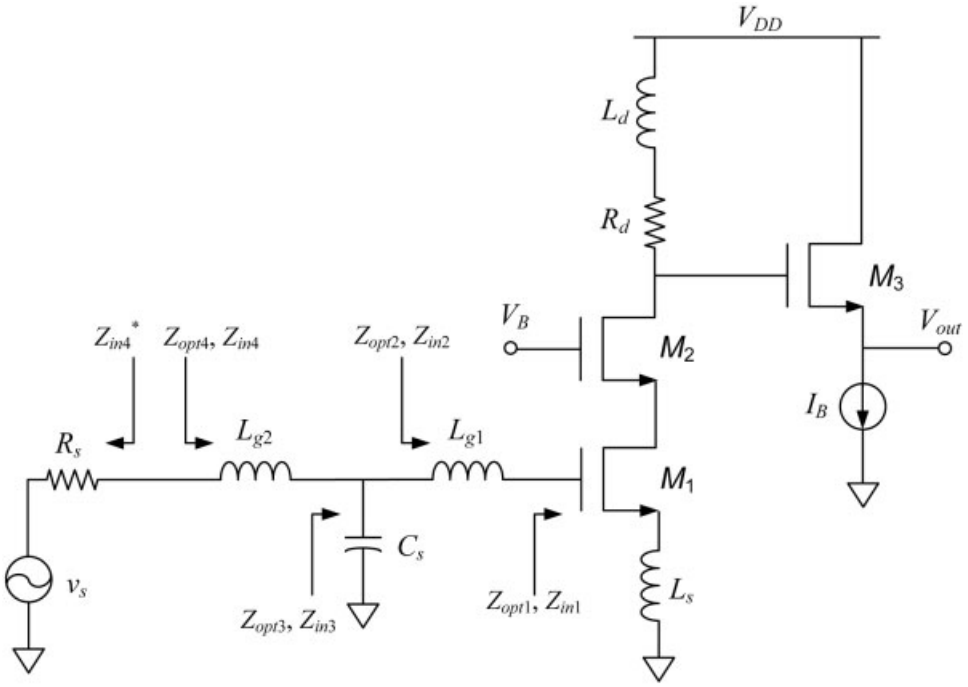

Figure 3 Proposed 3–5 GHz SNIM UWB LNA schematic

frequency in both directions. However, in Figure 2(a), over the frequency range of 3–5 GHz, which is the group-1 UWB band [4], the two curves are still in close proximity. Table 1 shows the values of Z_{in1}^* and Z_{opt1} at 3, 4, and 5 GHz. Because of this proximity, from the simulations it can be shown that the impedance matched to Z_{opt1} can provide more than 15 dB of matching to Z_{in1} at 3 and 5 GHz. This indicates that over the limited range of frequencies, say 3–5 GHz range, the wide band matching circuit for Z_{opt1} can satisfy the matching for Z_{in1} as well. Therefore, contrary to the initial observations as discussed above, this opens up the possibility of the ultra wide simultaneous noise and input matched LNA design.

For the UWB impedance matching, the adoption of band pass filter topology is popular [2, 3]. Figure 3 shows the complete schematic of the proposed UWB LNA schematic, which includes the band pass filter type input matching circuit and the output parts. In Figure 3, R_d and L_d represent the conventional resistive loading with inductive peaking, and the output buffer (composed of M_3 and I_B) is added for measurement purpose only. The L_{g1}, C_s, and L_{g2} in Figure 3 constitute the wide band matching circuit between the source impedance (in this case $R_s = 50\ \Omega$) and Z_{opt1}. The step by step selection for the values of L_{g1}, C_s, and L_{g2} and the corresponding change of Z_{opt} and Z_{in}^* are shown in Figures 2(b)–2(d), respectively. In Figures 2(b)–2(d), the values of L_{g1}, C_s, and L_{g2} are initially adjusted to make $\mathrm{Im}[Z_{opt2}] = 0$, $\mathrm{Re}[Z_{opt3}] = 50\ \Omega$, and $\mathrm{Im}[Z_{opt4}] = 0$, respectively, at 4 GHz. In that case, the LNA shown in Figure 3 becomes simultaneously noise- and input-matched at 4 GHz. Then, the values of L_{g1}, C_s, and L_{g2} are tweaked in such a way that the final curve of Z_{opt4} is located in close proximity to the 50-Ω point of the Smith Chart, like a circle as shown in the Figure 2(d). Since Z_{opt4} in Figure 2(d) does not exactly fall on 50 Ω over the frequency range of 3–5 GHz, the final NF of the UWB LNA is not exactly equal to the minimum NF (NF_{min}) of the cascode amplifier. However, because of the closeness of Z_{opt4} to 50 Ω, the noise figure

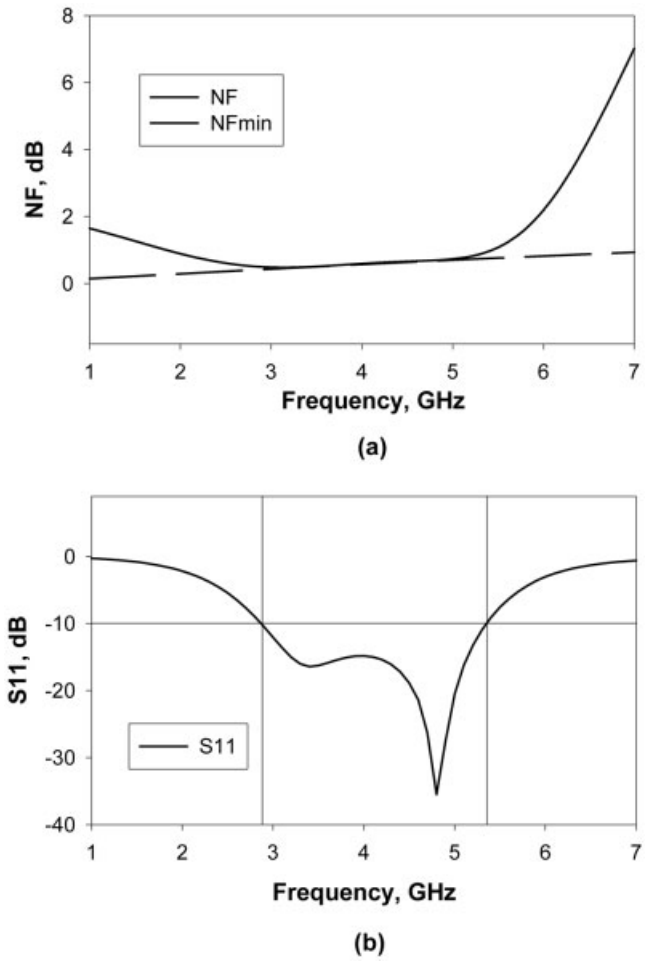

Figure 4 Simulated performance of the UWB SNIM LNA (a) NF and NF_{min} (b) $S11$

degradation from NF_{min} can be very small, especially when the cascode amplifier is designed for small values of noise resistance. The noise resistance of the cascode amplifier can be reduced by increasing the g_m of the transistor M_1 [1]. Note also that, in Figure 2(d), the corresponding Z_{in4}^* is located close enough to 50 Ω providing acceptable input impedance matching as well. Therefore, based on the design process as described above, it can be said that a UWB LNA can be designed to satisfy the pseudo-SNIM condition. Figure 4 shows the simulated NF and the input return loss of the proposed UWB LNA shown in Figure 3. As can be seen in Figure 3, the NF is nearly equal to NF_{min}, and the input return loss is greater than 10 dB over the frequency range of 3–5 GHz.

3. MEASUREMENT RESULTS

The UWB LNA shown in Figure 3 is implemented in 0.18 μm technology and dissipates 4 mA, excluding buffer, from 1.8 V supply. In the implemented LNA, contrary to the simulations shown in Figure 4, the on-chip matching components (L_{g1}, C_s, and L_{g2}) are used and the measurements are done by the on-wafer probing. The adoption of the on-chip inductors predicts significantly higher NF than what is shown in Figure 4.

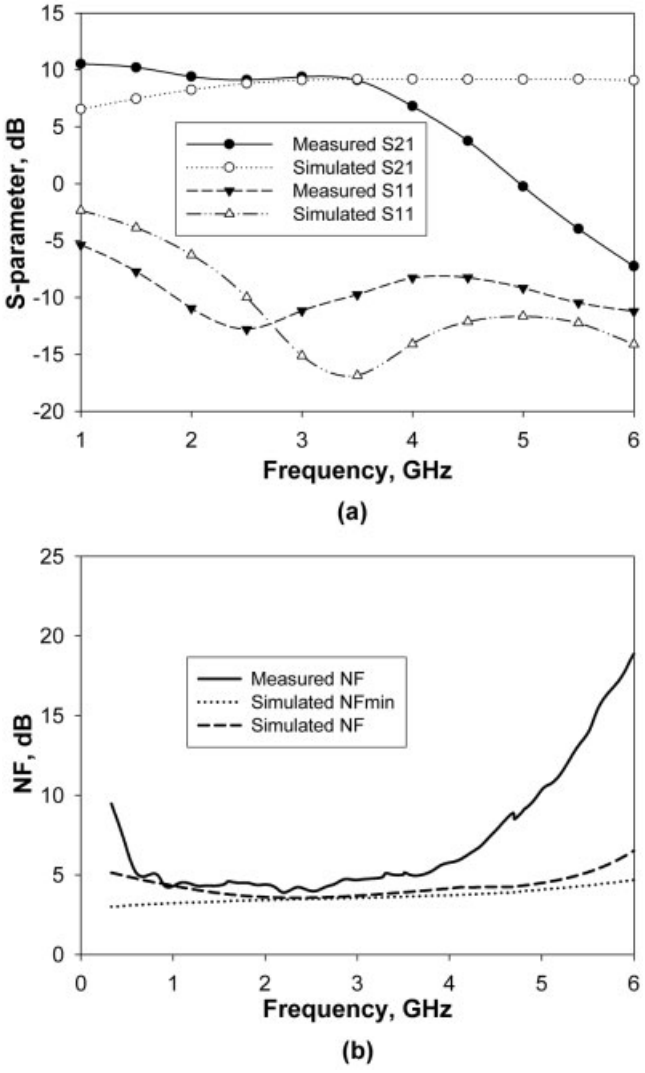

Figure 5 Measured and simulated performance of the proposed UWB SNIM LNA (a) *S*21 and *S*11 (b) NF and NF_{min}

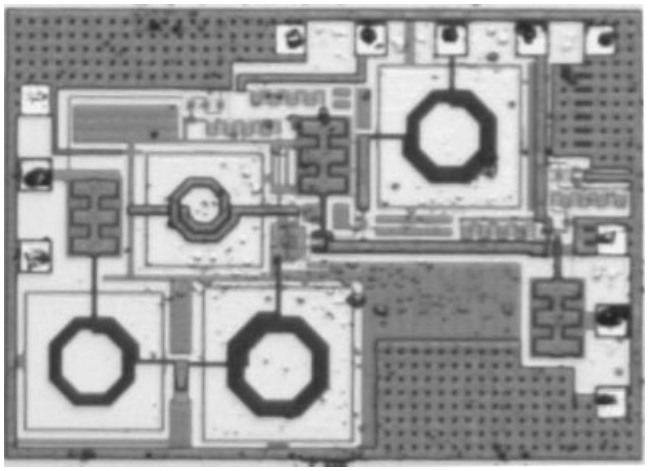

Figure 6 The chip micrograph of the fabricated UWB LNA

Figure 5 shows the measured and simulated gain (*S*21), input return loss (*S*11), and NF and NF_{min} as a function of frequency. In Figure 5, the measured and simulated values of *S*21 and *S*11 show considerable discrepancy at frequency higher than 4 GHz. The discrepancies can be referred to the inaccuracies of the component model at high frequencies, especially the bond pad. Because of the exclusion of the bond pad parasitic in the simulation, the measured result shows early gain drop at frequencies higher than 4 GHz. The gain reduction at high frequencies led to the corresponding premature increase in the measured NF in Figure 5(b). Overall, the implemented chip shows greater than 8 dB of return loss, maximum gain of 10.5 dB, and NF of 3–6 dB over the frequency range of 2–4 GHz. In spite of the discrepancy between the measurement and the simulation, the measured results support the proposed idea of UWB SNIM LNA design technique. Figure 6 shows the chip micrograph of the implemented LNA where the size is 820 × 1200 μm^2.

4. CONCLUSION

This paper reports a UWB LNA design technique that satisfies the simultaneous noise and input matching condition. The article analyses and identifies the fundamental limitation of the narrow band SNIM technique for the UWB application. By investigating the frequency behavior of the optimum source impedance and the complex conjugate of the input impedance of a cascode topology, the authors present a pseudo-SNIM UWB LNA design technique along with principles. A simultaneously noise- and input-matched UWB LNA is implemented in 0.18 μm CMOS technology and measurements show higher than 8 dB of input return loss, maximum gain of 10.5 dB, and noise figure of 3.9–6 dB over 2–4 GHz while dissipating 4 mA from a 1.8V supply. The measured results support the proposed concept of pseudo-SNIM UWB LNA design technique.

ACKNOWLEDGMENT

This work was supported in part by MOST/KOSEF (Intelligent Radio Engineering Center) under the SRC/ERC Program.

REFERENCES

1. T.-K. Nguyen, C.-H. Kim, G.-J. Ihm, M.-S. Yang, and S.-G. Lee, CMOS low noise amplifier design optimization techniques, IEEE Trans Microwave Theory Tech 52 (2004), 1433–1442.
2. A. Bevilacqua and A. Niknejad, An ultra-wideband CMOS LNA for 3.1

to 10.6 GHz wireless receivers, Int Solid State Circuits Conf Tech Dig, February 2004, 139–140.
3. A. Ismail and A. Abidi, A 3 to 10 GHz LNA using a wideband LC-ladder matching network, Int Solid State Circuits Conf Tech Dig, February 2004, 384–385.
4. Revision of Part 15 of the Commission's rules regarding ultra wide-band transmission systems. Federal Communications Commission [Online]. Available: http://www.fcc.gov/Document Indexes/Engineering Technology/2002 index OET Order.html.

MICROSTRIP ARRAY ANTENNA FOR FIRE-DETECTION APPLICATIONS

L. Vincetti, A. Polemi, and M. Zoboli
Department of Information Engineering, University of Modena and Reggio Emilia, Via Vignolese 905, 41100 Modena, Italy

Received 22 February 2007

ABSTRACT: *In this paper, a first investigation on critical issues for a fire-detection ground-based Ku-band radiometer antenna design is addressed. A printed technology with standard dielectrics has been employed, to reach low cost, simplicity in realization, and easy integrability with the electronic front-end. The antenna has been designed as an array of patches, where number of elements, spacings, and feeding currents has been optimized to fulfill requirements of low side lobe level and good crosspolarization. For the radio frequency front-end, the receiver architecture is a direct-conversion topology, because it is well suited to be monolithically integrated in a single chip.* © 2007 Wiley Periodicals, Inc. Microwave Opt Technol Lett 49: 2279–2282, 2007; Published online in Wiley InterScience (www.interscience.wiley.com). DOI 10.1002/mop.22649

Key words: *microstrip array antennas; radiometer; fire detection*

1. INTRODUCTION

Microwave radiometers (MRs) are widely employed on satellite/aircraft installations for remote sensing of the earth. In the industry, radiometers can be used for remote measurement of temperatures in ovens, converters, and other places where the use of conventional contacting temperature sensors or infrared cameras is impossible because of high temperatures, smoke, or water vapor. However, MRs can often not compete with these conventional sensors, which are in general cheaper and simpler to build. Nevertheless, recently they have been started to be employed in fire detection [1] [2], where MRs offer several advantages with respect to the well-established Infra-Red (IR) technology [3]. The microwave signals penetrate all materials, except of metals, allowing detection also through thick smoke and vapor, and making the measurement less sensitive to environmental conditions. The thermal microwave noise radiation comes from a thicker surface layer than the infrared radiation does. In contrast, the longer wavelength, compared to IR systems, reduces the spatial resolution, but contemporarily the higher frequency requires a more expensive electronic front-end. Consequently, antenna and Radio Frequency (RF) front-end must be properly designed and calibrated. In particular, the application to ground-based wildfire detection in forest environment is here investigated.

In these contests, the antenna design plays a key role. Its internal temperature and directivity pattern drastically affect the receiver front-end sensitivity. In particular, maximum directivity, narrow beamwidth, and low side lode level (SLL) are desirable features, to reduce unwanted signals and relax the noise figure (NF) of the low noise amplifier (LNA). For these reasons, parabolic reflectors have been employed in the past, but recently also microstrip array antennas have been investigated as good candidates to accomplish the above requirements. In this work, a patch array antenna for a wildfire detector operating at 13 GHz is optimized for ground-based applications. This goal is pursued in the framework of a national Italian university research program. To fulfill the overall requirements, the antenna specs have been defined from the RF electronic demands, for which analogs sections are integrated on a single chip based on 90 nm CMOS technology. As discussed later, the antenna design has started from a simple uniform array configuration, to set the more appropriate feeding technique and choose dielectric materials [4, 5]. This can also give a first rough inspect on the radiometer efficiency. Then, a suitable tapering has been introduced to reach the desired SLL; this reduces power accepted through minor lobes [6, 7]. This aspect is of primary importance in the present application, where the antenna can be placed also closed to the terrain. Thus, eventual unwanted radiations can affect the overall performance of the system.

This paper is organized as follows. A first section summarizes the typical radiometric concepts which are joined to the antennas parameters. Then, the design is described, by starting from the choice of single antenna element, and carrying on the feasibility study about the array. Finally, some first numerical results demonstrate the performance of the so designed microstrip array antenna.

2. RADIOMETRY AND ANTENNA PARAMETERS

In general, a body at temperature $T > 0$ K emits electromagnetic radiation with a power $P(f, T, \theta, \phi)$ in a certain direction of space θ, ϕ, and frequency f. In [2], some results for microwave emissions of different known materials involved in forest fires are shown. Referring to a typical scenario shown in Figure 1, let us now consider now an antenna with effective area A_{eff}, receiving power from a body in the direction θ, ϕ. The received power can be expressed in terms of the brightness temperature at the antenna [8] as

$$P_{\text{R}}(f,T,\theta,\phi) = \frac{1}{2}A_{\text{eff}}2k\frac{\Delta f}{\lambda^2}\int_{4\pi}|F(\theta,\phi)|^2 T(f,\theta,\phi)\, d\Omega \qquad (1)$$

which includes the normalized antenna pattern $F(\theta, \phi)$ [9] and the standard definition of antenna temperature T_{ant}

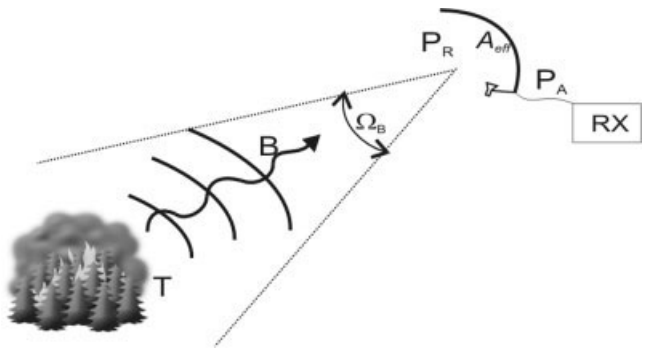

Figure 1 Typical scenario in the fire detection through passive radiometer antennas